Available online at www.CivileJournal.org

Civil Engineering Journal

(E-ISSN: 2476-3055; ISSN: 2676-6957)

Vol. 12, No. 05, May, 2026

Behavior of Rocket Piles Embedded in Sand under Static and Quasi-Static Cyclic Loading

Mohamed Elsiragy [1*], Waseim Azzam [2], Ali Basha [3]

[1] Department of Civil Engineering, Faculty of Engineering, October 6 University, Cairo 12585, Egypt.

[2] Department of Structural Engineering, Faculty of Engineering, Tanta University, Tanta, Egypt.

[3] Civil Engineering Department, Faculty of Engineering, Kafrelsheikh University, Kafrelsheikh City 33511, Egypt.

Received 09 June 2025; Revised 17 April 2026; Accepted 22 April 2026; Published 01 May 2026

Abstract

Pile foundations used in marine and onshore structures are often exposed to repeated axial loading, which can reduce their capacity and increase settlement over time. To address this issue, this study aims to evaluate the performance of rocket piles in sand and to understand how modifying pile geometry can enhance axial capacity under both static and quasi-static cyclic loading. A series of 1-g physical model tests were carried out to investigate the influence of sand relative density, pile slenderness ratio (L/D), fin-length ratio (Lf/L), fin-width ratio (b/D), fin location along the shaft, and surface roughness (Ra) on load–settlement behavior. The experimental results show that adding fins to the pile shaft significantly increases ultimate load capacity and reduces settlement compared to conventional smooth piles. The improvement is particularly noticeable under quasi-static cyclic loading, where fins help mobilize greater shaft resistance and limit the accumulation of settlement. Furthermore, larger fin-width and fin-length ratios provide greater performance enhancement. The main contribution of this study is the experimental evaluation of rocket piles under cyclic conditions and the development of practical design charts that allow engineers to estimate load improvement and settlement reduction based on fin geometry and surface characteristics, offering a more economical and efficient foundation solution in sandy soils.

Keywords: Experimental Study; Rocket Pile; Sand; Surface Roughness; Static Load; Quasi-Static Cyclic Loading.

1. Introduction

Pile foundations are widely used to support structures subjected to various types of loading, including axial, lateral, uplift, and cyclic loads. Different pile types such as steel pipe piles, H-piles, screw piles, enlarged-base piles, bladed piles, and finned piles have been developed to improve load-carrying capacity and performance. Consequently, numerous studies have investigated pile modification techniques aimed at enhancing shaft resistance and end-bearing capacity by altering pile geometry at specific depths along the shaft. Earlier research demonstrated that modifying pile shape into tapered or pyramidal forms can improve axial response and stress distribution [1, 2].

One of the more recent developments in pile modification is the *rocket pile*, which consists of a conventional monopile fitted with four radial plates (fins) arranged at 90° intervals around the shaft [3]. Most previous studies on finned or rocket piles have primarily focused on lateral and uplift resistance, evaluating the contribution of fins in improving lateral load capacity and overturning resistance. However, limited attention has been given to their axial behavior, particularly under cyclic loading conditions. Understanding pile response under static and cyclic axial

* Corresponding author: mohamed.nabil.eng@o6u.edu.eg

https://doi.org/10.28991/CEJ-2026-012-05-013

loading is a fundamental issue in geotechnical engineering. Offshore and coastal structures such as wind turbines, marine platforms, silos, and transmission pylons are frequently subjected to repeated loading from waves, wind, and operational forces. The cyclic response of displacement piles in sand depends on several factors, including load amplitude, load history, embedded length, sand properties, number of cycles, and loading frequency [4, 5].

Poulos (1981, 1988) [6, 7] demonstrated that cyclic loading leads to progressive stiffness degradation and reduction in shaft resistance, and introduced the concept of cyclic stability zones based on mean and cyclic load levels. Although design standards acknowledge the importance of cyclic loading, explicit procedures for evaluating cyclic pile performance are often lacking. Experimental and numerical studies on plain piles [8-10] confirmed that cyclic loading can induce friction fatigue and progressive reduction in shaft capacity. Other investigations have examined installation [11] and dynamic response of piles supporting wind turbines [12-14], highlighting the influence of cyclic degradation on foundation stiffness.

In parallel, several researchers proposed geometric modifications such as fins or wings to enhance uplift, lateral, and torsional performance [15-20]. Their results demonstrated a significant increase in tension, lateral, and torsional capacities when fins were incorporated at the pile toe. Notably, optimizing the fin width to match the pile diameter and setting the inclination angle (β) to 90° resulted in notable enhancements in uplift capacity, reaching up to 1.82, 3, and 6 times that of a normal pile with stiffness ratios (L/D) of 15, 20, and 30, respectively. Moreover, a novel technology for pile modification involving the use of wings along the pile at specific depths was introduced as an experimental investigation by Sakr et al. [21]. On the other hand, These studies reported significant improvements in tension and lateral capacities when fins were installed at the pile toe. However, despite these advances, the axial cyclic behavior of rocket piles embedded in sand remains insufficiently investigated. The limited investigation of such approach has been done by Hagemann et al. [22] and Zhou et al. [23]. In particular, the influence of fin geometry, surface roughness, fin location along the shaft, and cyclic loading rate on axial performance is not well established. Existing empirical methods for plain piles may not be directly applicable to rocket piles due to their altered load transfer mechanism.

While previous studies have extensively explored lateral and uplift behavior of finned or rocket piles, there is a clear gap in understanding their vertical response under cyclic axial loading. The interaction mechanism between fins, surrounding sand, and cyclic shaft resistance degradation has not been systematically examined. Moreover, the applicability of existing design recommendations to rocket piles remains uncertain. Therefore, the objective of this study is to experimentally investigate the axial behavior of single rocket piles embedded in sand under static and quasi-static cyclic loading. The research aims to evaluate the efficiency of fins in enhancing axial capacity and reducing settlement compared to plain piles, while examining the influence of key parameters such as relative density, slenderness ratio (L/D), fin length ratio (Lf/L), fin width ratio (b/D), fin position, and surface roughness. The ultimate goal is to provide a clearer understanding of the cyclic soil–pile interaction mechanism and contribute toward improved design guidance for modified piles in sandy soils. The investigated parameters are;

- Slenderness ratio (L/D),
- Fin-length ratio (Lf/L),
- Fin-width ratio (b/D),
- Fin position, and
- Surface roughness (Ra).

The paper structures contain the following sections of parts. Section 2 presents the experimental testing program, detailing the test setup, model preparation, material properties, instrumentation, and loading techniques. Section 3 outlines the testing strategy and studied parameters. The results under static loading conditions are discussed in Section 4, followed by an analysis of the quasi-static cyclic behavior, with particular emphasis on the effects of fin geometry and surface roughness on load capacity and settlement. Also, it provides a comparative evaluation between rocket piles and conventional plain piles and introduces practical design charts derived from the experimental results. Section 5 shed the light in the problem of scale effect. Finally, section 6 summarizes the main findings and conclusions of the present research.

2. Experimental Program

The following flowchart in Figure 1 illustrates the workflow and briefly presents the methodology process.

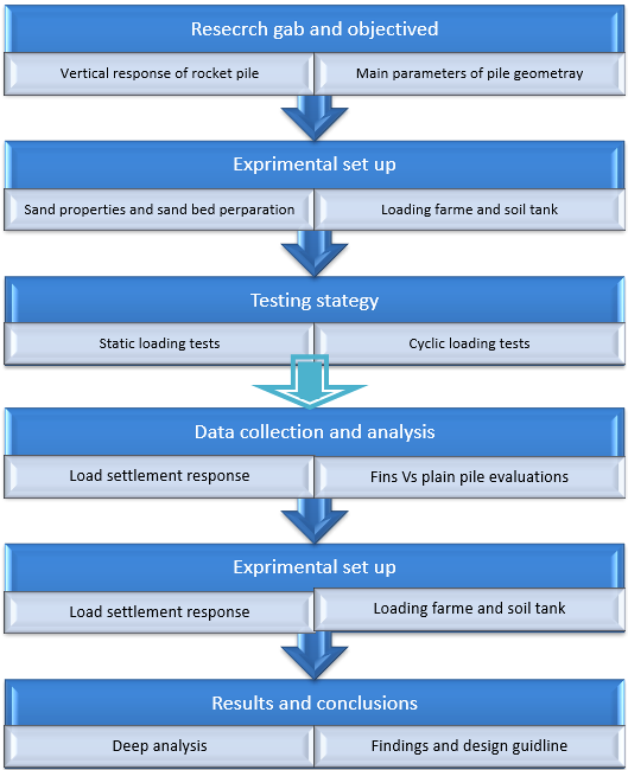

Figure 1. Flow chart of the investigated process and methodology

2.1. Tested Sand and Properties

A well-graded silica sand, classified according to ASTM D422-63 [24], was used in the experimental program. Based on ASTM D3080/D3080M-11 [25], direct shear box tests were conducted at a relative density of 85% to determine the shear parameters of the tested soil samples. The internal friction angle was found to be 35°. The sand was placed in layers with compaction effort; each layer had a thickness of 50 mm, and a manual compactor with a weight of 30 N was used to achieve the required relative density, as described by Sakr et al. [26] and Basha & Azzam [27].

2.2. Loading System and Test Model

A schematic of the steel loading system and soil testing model is shown in Figure 2. The tank consists of a cylindrical cell with an internal diameter of 315 mm and a height of 850 mm. The tank dimensions satisfy the scale effect requirements [28]. The loading frame includes top and bottom plates, four solid steel rods, a two-way air piston, and a compressor to generate the required air pressure to move the piston. Four dial gauges with a precision of 0.002 mm were used to measure the vertical displacement of both the soil surface and the modeled pile.

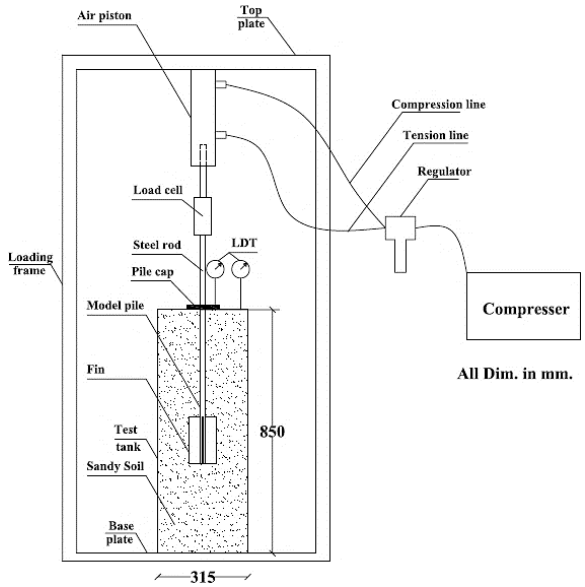

Figure 2. Schematic diagram of the model test

2.3. Typical Piles and Execution Technique

The piles were modeled using solid steel rods with a modulus of elasticity of 2.10×10^5 MPa and a diameter of 17 mm. The fins were fabricated from steel sheets with a thickness of 2 mm and a modulus of elasticity of 2.15×10^5 MPa. Figure 3 presents a schematic diagram of the modeled pile with three different fin positions. The modeled piles and fins were coated with a layer of epoxy, and fine sand with a diameter of 0.15 mm, equal to the median particle size, was sprinkled over the epoxy layer to achieve appropriate pile–soil interaction [29, 30]. The ratios (L/D) of the test piles were 10, 15, 20, and 25. A non-displacement technique with an undisturbed process was used as the installation method.

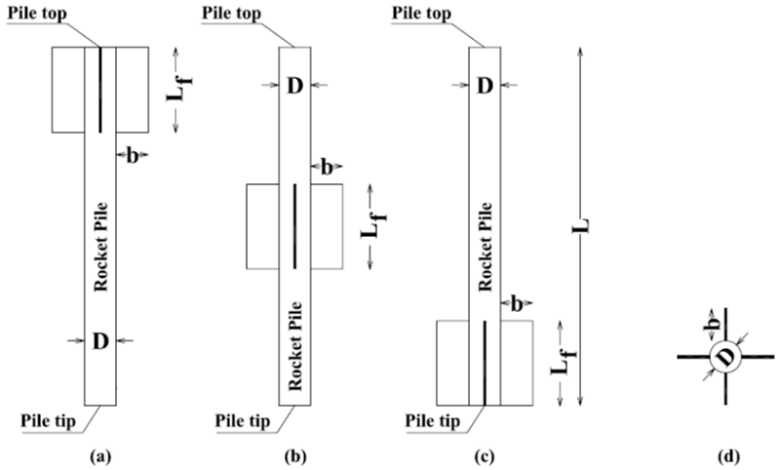

Figure 3. Study variables of finned piles: (a) top fin pile; (b) middle fin pile; (c) tip fin pile; (d) plan section of finned pile

2.4. Testing Approach and Strategy

The studied and testing parameters are shown in Tables 1 and 2, which specify the procedures that were adopted in this research with suggested testing parameters. Table 2 shows the static load test program and all test series. While Table 3 mentions repeated variable loading (cyclic tests).

Table 1. Model tests program under static load

Group	Fin position w.r.t pile	Fin length ratio L_f/L	Fin width ratio b/D	Pile surface roughness R_a mm	Slenderness ratio L/D	Installation method / relative density	Test No
I	-	-	-	Smooth	10, 15, 20, 30	Non-displacement Dr =85%,	4
II	-	-	-	0.075, 0.15, 0.425	10, 15, 20, 30		12
III	At Top	0.10, 0.15, 0.20	0.50, 1.0, 1.50	0.075, 0.15, 0.425	20		12
	At Middle	0.10, 0.15, 0.20	0.50, 1.0, 1.50	0.075, 0.15, 0.425	20		12
	At Tip	0.10, 0.15, 0.20	0.50, 1.0, 1.50	0.075, 0.15, 0.425	20		12

Table 2. Repeated variable loading cases

Loading case	b/D	P_{min} (N)	P_{max} (N)	$P_{u, static}$ (N)	$P_{u, cyclic}$ (N)	$P_{max}/P_{u, static}$	$P_{max}/P_{u, cyclic}$	% P_u
(1)	0.50	0.0	400	1257	1455	0.318	0.275	15.75
(2)	1.00	0.0	400	1375	1610	0.290	0.248	17.10
(3)	1.50	0.0	400	1492	1780	0.268	0.224	19.30

3. Results

3.1. Results of Static Load Test

The main purpose of the static load test is determining the maximum load capacity of the tested pile under different slenderness ratios and different surface roughness. The load settlement relationships of a pile with and without fins are presented in the following sections. The definition of the failure ultimate load capacity of the pile is determined from the load-settlement charts at the steeper part of the curve. In case of absence of a clear inflection point of the load settlement curve, the ultimate load capacity of the pile is determined to be equivalent to the settlement of 10% of the pile diameter. The determination of ultimate capacity (Pu) utilized a hybrid methodology to capture both geometric and structural failure thresholds. Initially, the 10% diameter settlement rule was employed, following the classical recommendations of Terzaghi [31] and the codified standards in ASTM D1143 [32] and Eurocode 7. This provides a uniform benchmark for defining the ultimate limit state in displacement piles. Furthermore, to evaluate the specific stiffening effects of the finned geometry, the Tangent Method [33] was integrated. This second technique pinpointed

the inflection point where settlement rates accelerate sharply relative to load increments. This dual-layered analysis ensures that the observed benefits of finned configurations are validated against both serviceability requirements and theoretical stability.

3.1.1. Load-Displacement Diagrams for Static Test

First, the behavior of standard piles under vertical static load was examined to obtain essential reference data for meaningful comparison. The load–settlement relationships for piles without fins, at a relative density of 85%, for different surface roughness conditions and slenderness ratios (L/D), are shown in Figure 4.

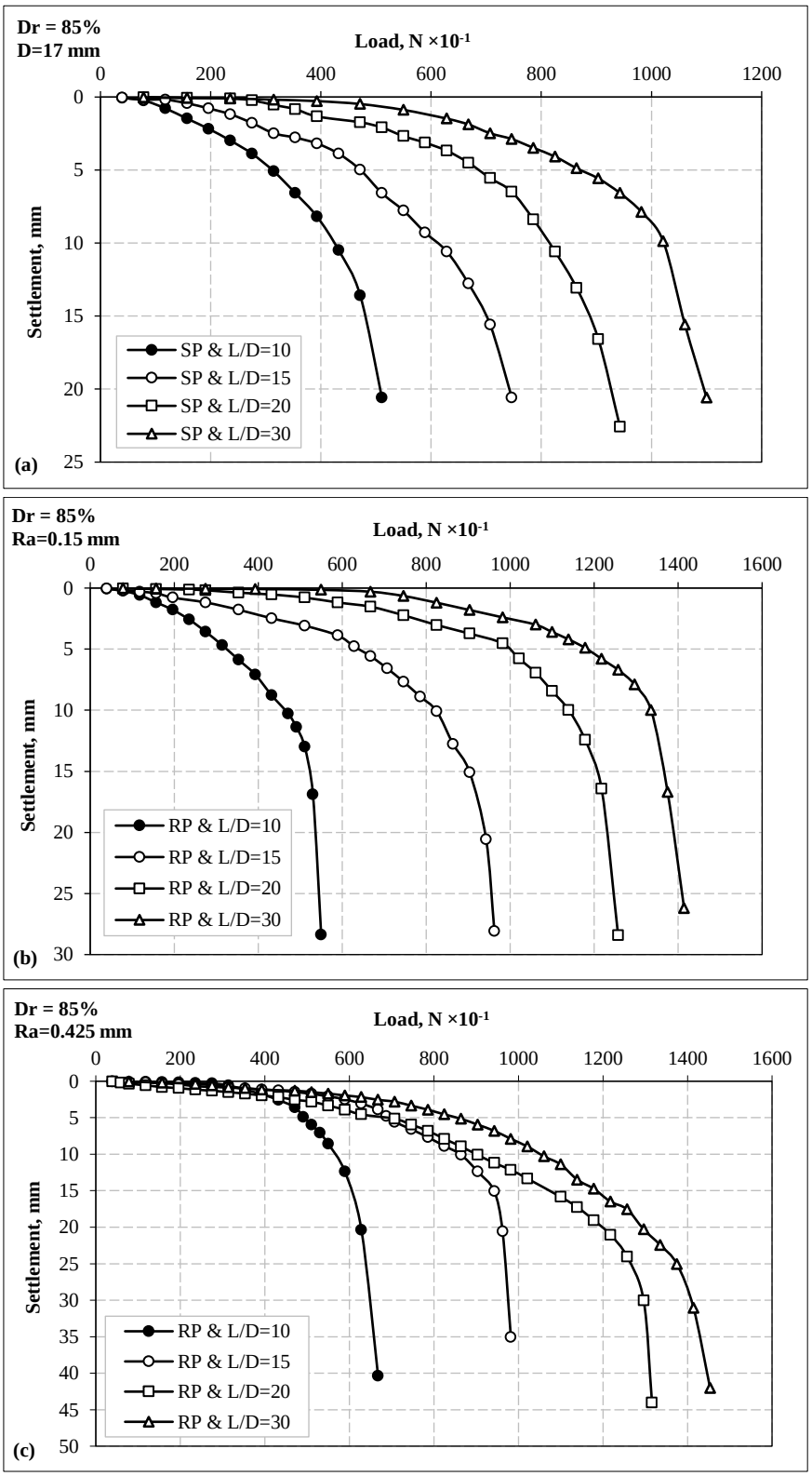

Figure 4. Load-settlement relationships for tested piles without fins at Dr = 85%:(a) smooth pile surface; (b) rough pile surface Ra =0.15 mm; (c) rough pile surface Ra =0.425 mm

The failure load is defined as the axial failure load for all test series. The ultimate load corresponds to the point on the displacement curve where displacement continues to increase at a constant load. For smooth pile surfaces, the ultimate loads were 510 N, 746 N, 942 N, and 1100 N corresponding to L/D ratios of 10, 15, 20, and 30, respectively, as shown in Figure 4-a. For piles with an average surface roughness (Ra) of 0.15 mm, the ultimate loads were 550 N, 962 N, 1257 N, and 1414 N for L/D ratios of 10, 15, 20, and 30, respectively, as shown in Figure 4-b. For piles with an average surface roughness of Ra = 0.425 mm, the ultimate loads were 667 N, 982 N, 1316 N, and 1453 N corresponding to L/D ratios of 10, 15, 20, and 30, respectively, as shown in Figure 4-c. Overall, the ultimate load increases with increasing slenderness ratio and surface roughness.

The load–settlement curves are nonlinear and tend to become approximately parallel to the settlement axis at higher loads. A clear increase in the ultimate load is observed with increasing slenderness ratio and surface roughness. At the initial stage, the load–settlement curves are similar until the surrounding soil reaches its yield stress, after which the curves become nonlinear. Surface roughness affects the load–settlement behavior and enhances the ultimate load capacity. The linear portion of the curve increases with increasing surface roughness, particularly for shorter piles.

It can be concluded that the effects of surface roughness and L/D ratio are clearly illustrated in Figure 4, which establishes a baseline by examining piles without fins. The comparison includes smooth surfaces and two levels of roughness (Ra = 0.15 mm and Ra = 0.425 mm). Regarding the influence of L/D, in all three figures, as the L/D ratio increases (i.e., the pile becomes longer and more slender), the curves shift to the right, indicating that longer piles can support higher loads for the same settlement. In terms of surface texture, comparing Figures 4-a to 4-c shows that rough piles carry higher loads than smooth piles due to increased skin friction, as the rough surface provides better resistance against soil movement. Regarding settlement behavior, as the load approaches the ultimate capacity, the curves become steeper. Rougher piles exhibit a more gradual transition in the curve, suggesting a more stable load transfer mechanism before failure.

3.1.2. Effect of Fin Position on the Load-Settlement Curve

The effect of fin position on the ultimate pile load and the load–settlement curve was examined. The results clearly show that for L/D = 20, the optimal fin position is at the pile tip. Figure 5 presents the load–settlement relationships for a smooth pile with L/D = 20, b/D = 0.50, and Dr = 85% for different h/L ratios. For smooth piles with and without fins, as shown in Figure 5-a, the ultimate pile capacity of the SP-FB model at h/L = 0.10 increased by approximately 33.4%, 23.1%, and 14.3% compared to the SP, SP-FT, and SP-FM models, respectively. At h/L = 0.15, the ultimate pile capacity of SP-FB increased by about 66.7%, 51.0%, and 33.3% relative to SP, SP-FT, and SP-FM, respectively, as shown in Figure 5-b. At h/L = 0.20, the ultimate pile capacity of SP-FB increased by approximately 108%, 67%, and 56% compared to SP, SP-FT, and SP-FM, respectively, as illustrated in Figure 5-c.

At a constant fin width, increasing the h/L ratio leads to an increase in fin efficiency. For the SP-FB model, fin efficiency increased by approximately 25% and 56% at h/L = 0.15 and h/L = 0.20, respectively, compared to h/L = 0.10. For the SP-FM model, the increase was about 7% and 14% for h/L = 0.15 and h/L = 0.20, respectively. Similarly, for the SP-FT model, fin efficiency increased by approximately 2% and 15% at h/L = 0.15 and h/L = 0.20, respectively, relative to h/L = 0.10, as shown in Figures 5-a to 5-c. The results indicate that, at a constant fin width, the ultimate pile capacity increases with increasing h/L ratio. In general, as the ratio increases from 0.10 to 0.20 (i.e., longer fins), the load–settlement curves shift further to the right. The h/L = 0.20 case (Figure 5-c) shows the most significant improvement, nearly doubling the load capacity compared to the pile without fins. Additionally, piles with fins sustain higher loads before reaching the point of rapid settlement.

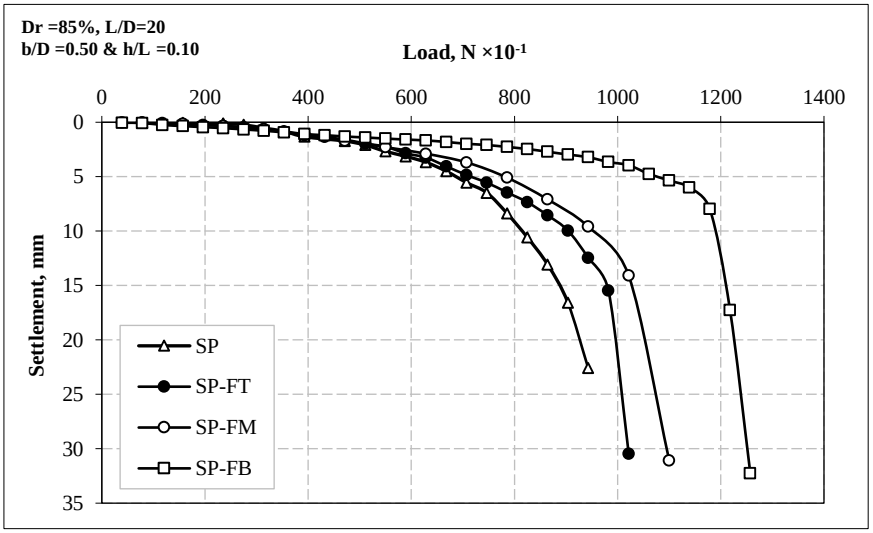

(a)

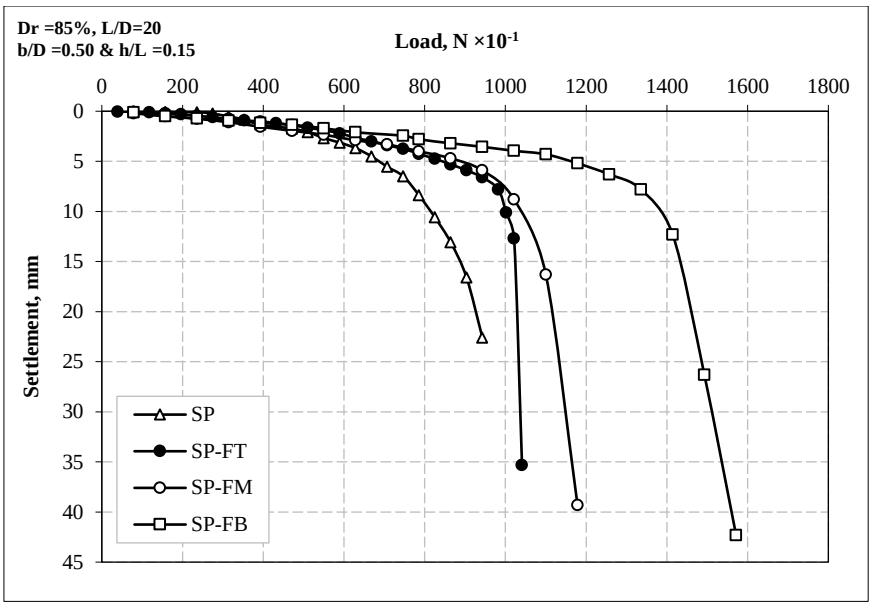

(b)

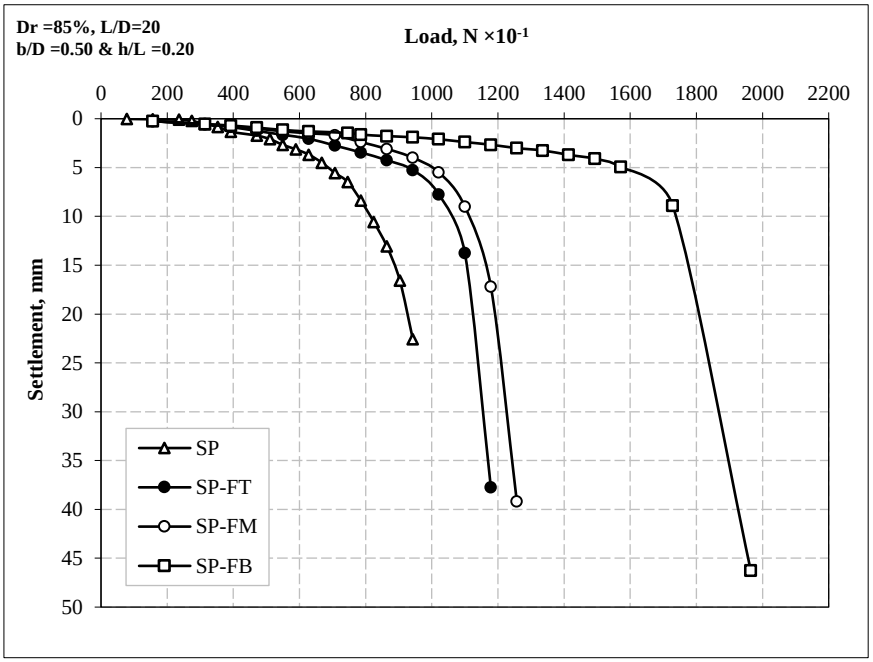

(c)

Figure 5. Load-settlement relationships for test piles with and without fins at Dr = 85%; L/D=20; b/D=0.50:(a) h/L=0.10; (b) h/L=0.15; (c) h/L=0.20

3.1.3. Effect of Fin Length Ratio on the Load-Settlement Curve

Figure 6 presents the load–settlement curves for piles with and without fins at a relative density of 85%, with L/D = 20 and b/D = 0.50, for three different fin positions: at the pile top, middle, and tip. The experimental results in Figure 6 show that the ultimate pile load increases with increasing fin length ratio. The lowest increase in ultimate capacity was observed when the fin was placed at the pile top, with increases of approximately 8.39%, 10.51%, and 25.0% for h/L = 0.10, 0.15, and 0.20, respectively, compared to the regular pile (SP), as shown in Figure 6-a. The highest increase in ultimate load occurred when the fin was positioned at the pile tip, with increases of about 33.44%, 66.77%, and 108.50% for h/L = 0.10, 0.15, and 0.20, respectively, as shown in Figure 6-c.

For fins placed at the pile middle, the increases were 16.70%, 25.0%, and 33.0% for h/L = 0.10, 0.15, and 0.20, respectively, as shown in Figure 6-b. These results indicate that placing fins at the pile tip is more effective, as it takes advantage of higher confining pressure at greater depths and increases the end-bearing area, making it more difficult for the pile to penetrate further into the soil.

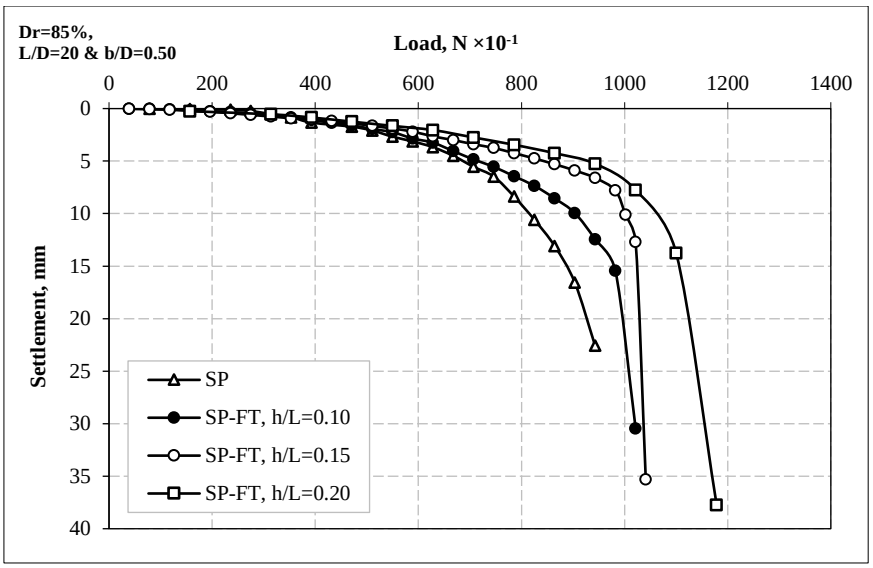

(a)

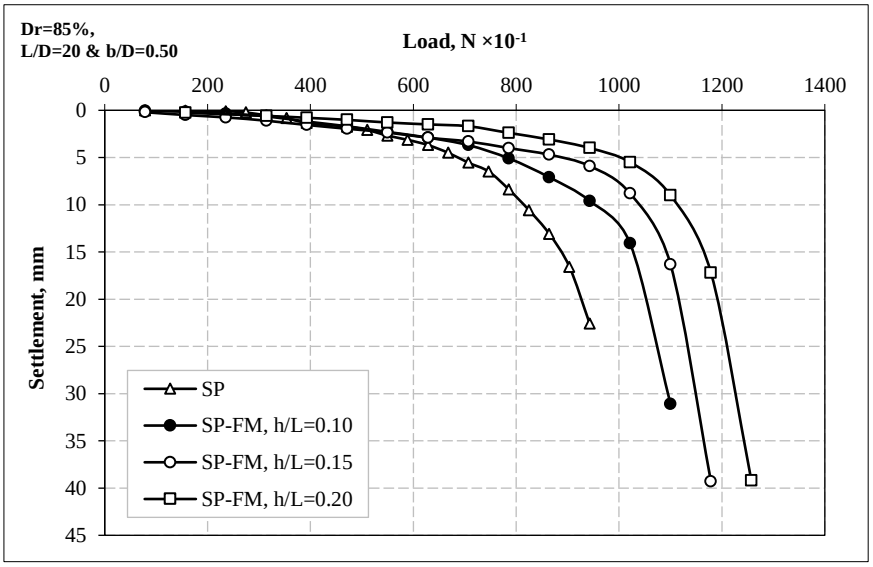

(b)

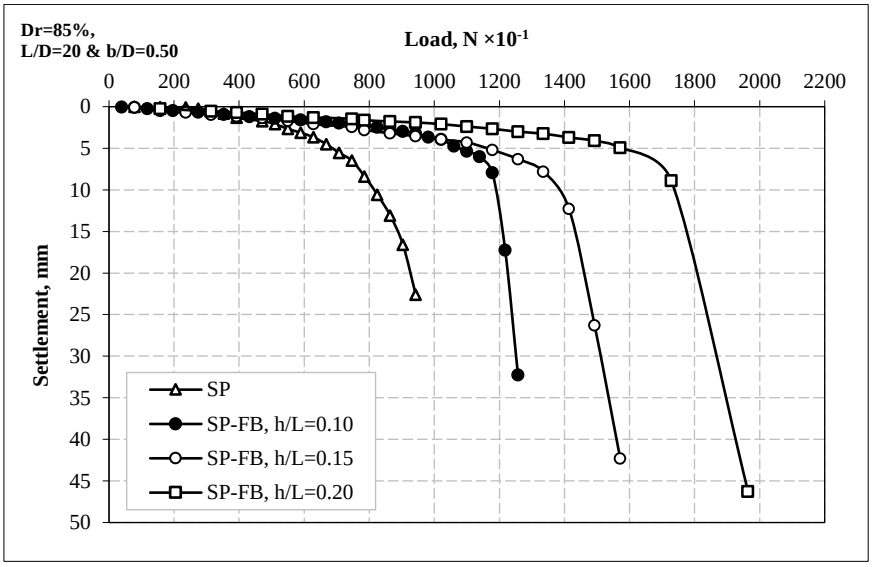

(c)

Figure 6. Load-settlement relationships for test piles with and without fins at Dr = 85%; L/D=20; b/D=0.50 for different fins positions :(a) fins at top; (b) fins at middle; (c) fins at tip

3.1.4. Effect of Fin width Ratio on the Ultimate Pile Capacity

The pile load capacity of a single pile with fins is significantly influenced by the fin width ratio. Figures 7-a to 7-c illustrate the variations in the increase of ultimate load capacity for different fin positions and fin-length ratios (h/L). For example, when h/L = 0.10, the ultimate load capacity increases by 8%, 17%, and 25% of its initial value for piles SP-FT, SP-FM, and SP-FB, respectively, as shown in Figure 7-a, with the fin width ratio varying from 0.50 to 1.50. Similarly, at h/L = 0.15, the increase ranges from 6% to 41% for the same piles, as illustrated in Figure 7-b. For h/L = 0.20, the increase ranges from 16% to 33%, as shown in Figure 7-c. However, for pile SP-FT at h/L = 0.10, 0.15, and 0.20, varying the fin width from 0.50 to 1.50 has a negligible effect on increasing the ultimate load capacity, as observed in Figures 6-a to 6-c and reflected in Figures 7-a to 7-c. In contrast, for all other fin positions, a noticeable improvement in ultimate load capacity is observed within the studied range. Therefore, it can be inferred that the optimal fin width ratio (b/D) lies at or above 1.0 to achieve maximum ultimate load capacity.

The experimental results show that increasing the fin width ratio enhances the ultimate load capacity due to the increase in fin width and the corresponding rise in overburden pressure acting on the fins. A larger fin width results in a greater confined soil volume between the fins, which increases the size of the equivalent cylindrical soil block and, consequently, enhances shear resistance. As a result, the load capacity of finned piles increases with higher fin width ratios. Conversely, as the fin width ratio decreases toward zero (i.e., a regular pile, SP), the confined soil volume between fins diminishes, reducing the equivalent cylindrical block size and ultimately lowering the load capacity until it approaches that of a regular pile.

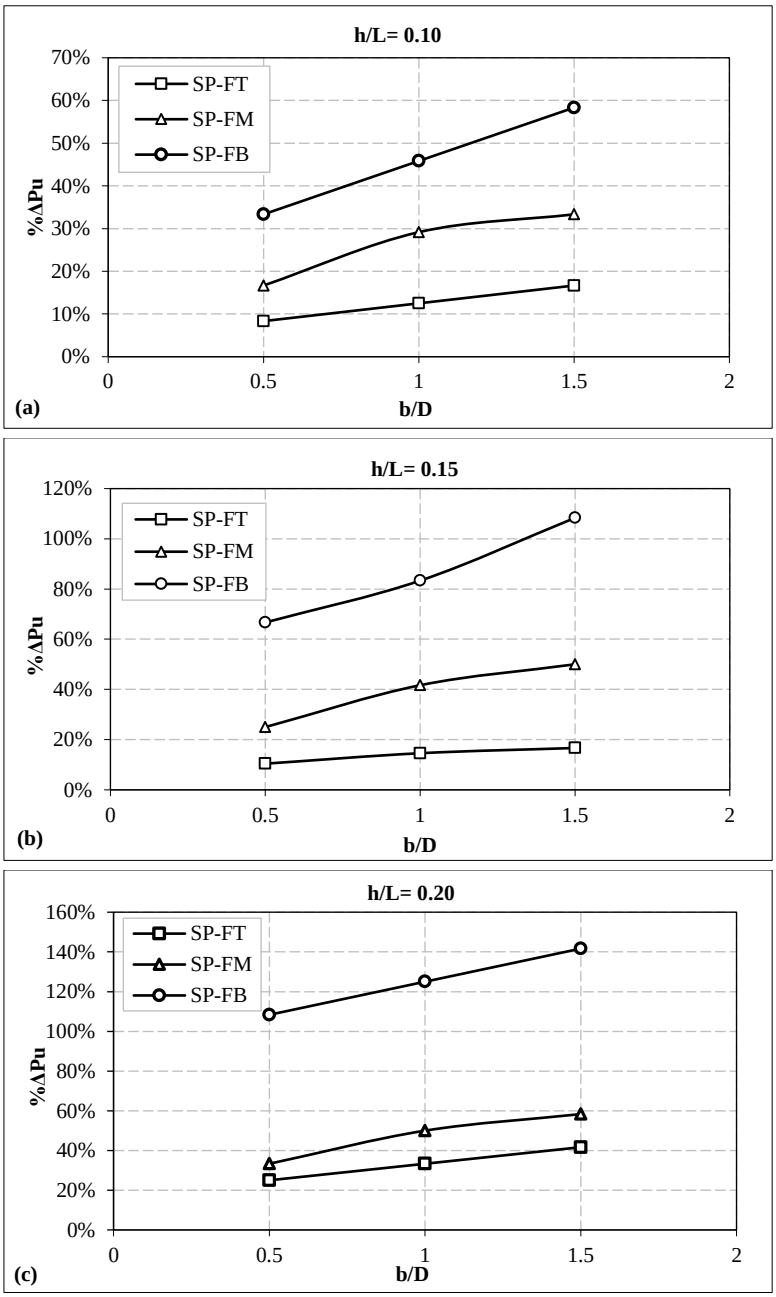

Figure 7. Variation of increase in ultimate load versus b/D for different fins position: (a) h/L =0.10; (b) h/L =0.15; (c) h/L =0.20

3.1.5. Effect of Slenderness Ratio and Surface Roughness on the Load Ratio

Pile surface roughness also has a significant effect on pile capacity. The effect of average surface roughness (Ra) with different slenderness ratios (L/D = 10, 15, 20, and 30) on the load ratio (Lr) is presented in Figure 8. The load ratio was calculated as the ratio of the ultimate pile load for a given case to that of the smooth pile (SP). The load ratio–surface roughness curves initially exhibit a linear trend and become nearly parallel to the horizontal axis at higher values. A clear increase in load ratio is observed with increasing slenderness ratio and surface roughness. As shown in Figure 9, the load ratio increases linearly with increasing surface roughness until reaching a peak at Ra = 0.08 mm.

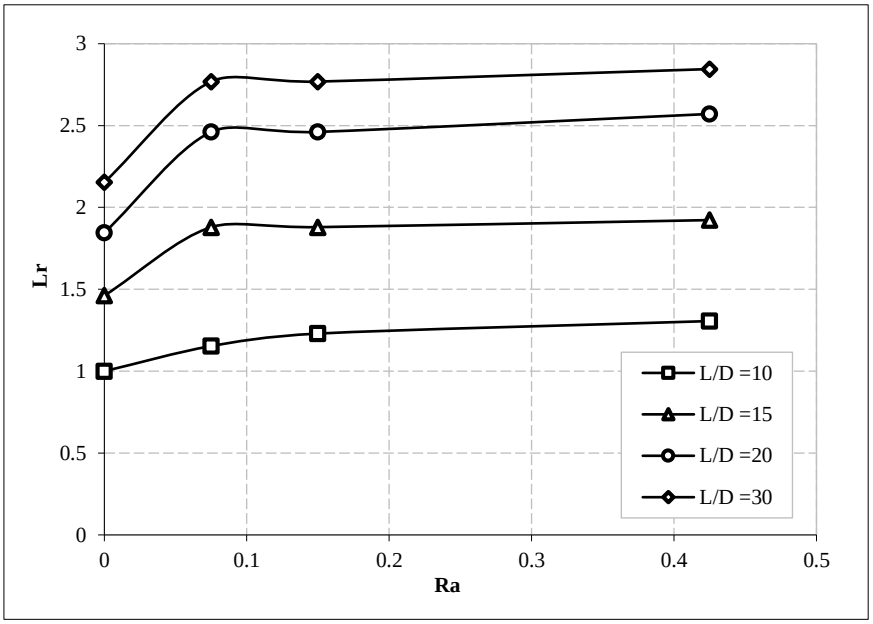

Figure 8. Variation of load ratio versus average surface roughness for different L/D

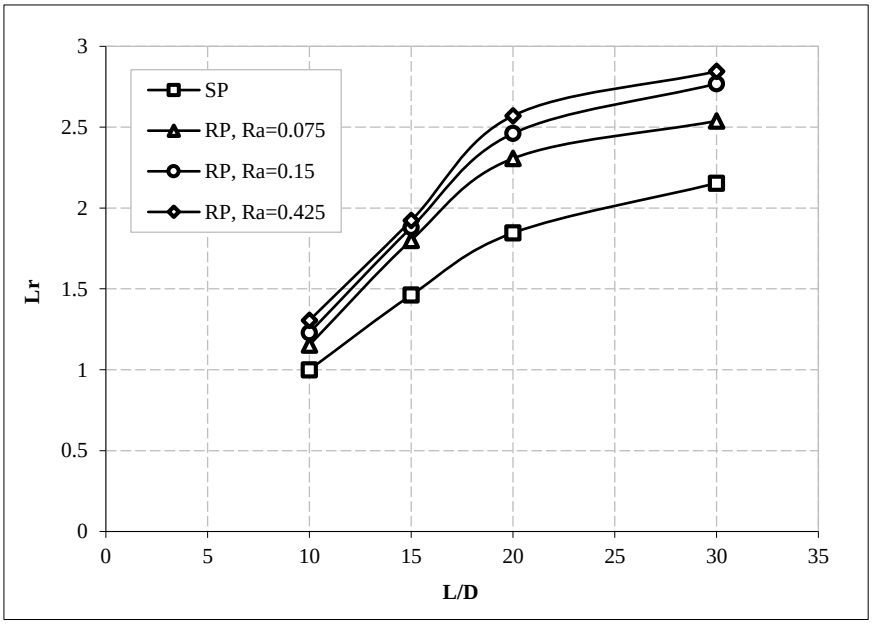

Figure 9. Variation of load ratio versus L/D for different surface roughness

3.2. Results of Quasi Static Cyclic Pile Load Test

3.2.1. Quasi Static Cyclic loading

The cyclic load was applied using a controlled two-way air piston, which exerted a reaction force against the pile top. The cyclic test procedure was carried out in the following sequence. After installation of the pile, the axial

compressive force was increased until reaching the mean static load (P_0). The load was then increased by the cyclic amplitude (A_0) to reach the maximum cyclic load (Pmax) within 60 seconds. Subsequently, the applied load was gradually decreased by $2A_0$ to reach the minimum load (Pmin) in 120 seconds. After that, the load was again increased gradually by $2A_0$to return to Pmax in another 120 seconds. These steps were repeated until 10 cycles were completed. According to Poulos [34], the significant effects of cyclic loading on piles embedded in sandy soil occur primarily within the first 10 cycles.

The applied load and the corresponding pile settlement at the pile cap were continuously monitored and recorded from the start of the initial loading through the 10 cycles until the ultimate pile capacity was reached. The duration of each force-controlled cycle was approximately 240 seconds.

The measured cyclic load was applied at the pile top during the cyclic tests. The value of the cyclic load was defined as follows:

$$P(t) = P_0 + \frac{A_0 sin(2ft)}{2} \quad (1)$$

where, P(t) is the cyclic load applied at the pile top, Po is the mean static load, Ao is the bounty of the cyclic load, f is the loading frequency, and t is the time (Figure 10). Table 3 summarizes all variable values used in the cyclic tests.

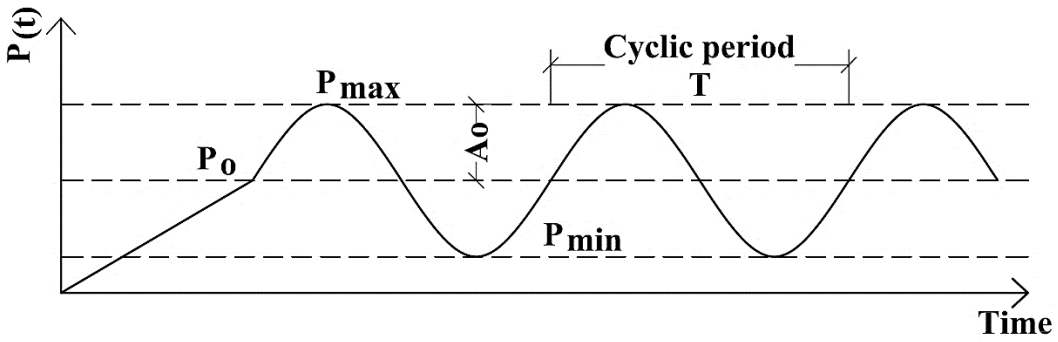

Figure 10. Cyclic loading characteristics

Table 3. Repeated variable loading cases

Loading case	b/D	P_{min} (N)	P_{max} (N)	$P_{u, static}$ (N)	$P_{u, cyclic}$ (N)	$P_{max}/ P_{u, static}$	$P_{max}/ P_{u, cyclic}$	% P_u
(1)	0.50	0.0	400	1257	1455	0.318	0.275	15.75
(2)	1.00	0.0	400	1375	1610	0.290	0.248	17.10
(3)	1.50	0.0	400	1492	1780	0.268	0.224	19.30

Figure 11 presents the variation in cyclic load–settlement behavior for ten cycles of a constant amplitude (400 N) under force-controlled loading, with the same relative density (Dr = 85%), slenderness ratio (L/D = 20), fin length ratio (Lf/D = 0.10), and varying fin width ratios. It is evident from Figure 11 that soil resistance under cyclic loading differs with changes in fin width ratios (b/D = 0.50, 1.0, 1.50), even under the same loading amplitude. As shown in Figures 11-a to 11-c, cyclic settlement decreases as the fin width ratio increases. The recorded cyclic settlements were 1.36, 1.07, and 0.91 mm for fin width ratios (b/D) of 0.50, 1.00, and 1.50, respectively, at the end of ten cycles. The reduction in cyclic settlement was approximately 26.5% and 33.0% for b/D = 1.00 and 1.50, respectively, compared to b/D = 0.50.

The unit side surface area of fins for b/D values of 0.50, 1.00, and 1.50 was 68 mm, 136 mm, and 204 mm, respectively. Accordingly, the increase in fin surface area followed ratios of 1, 2, and 3 for b/D values of 0.50, 1.00, and 1.50, respectively. Experimental results indicate that the side surface area of fins has a minor effect on cyclic response.

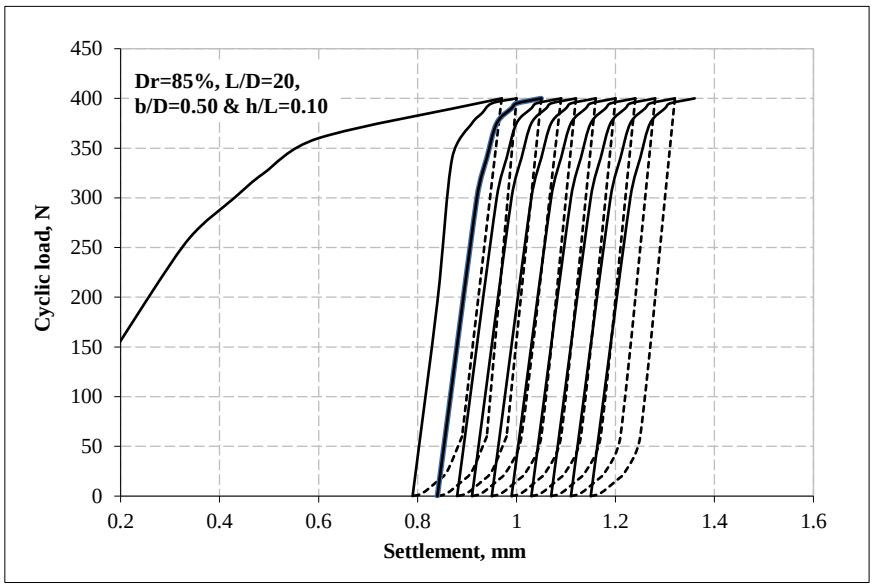

(a)

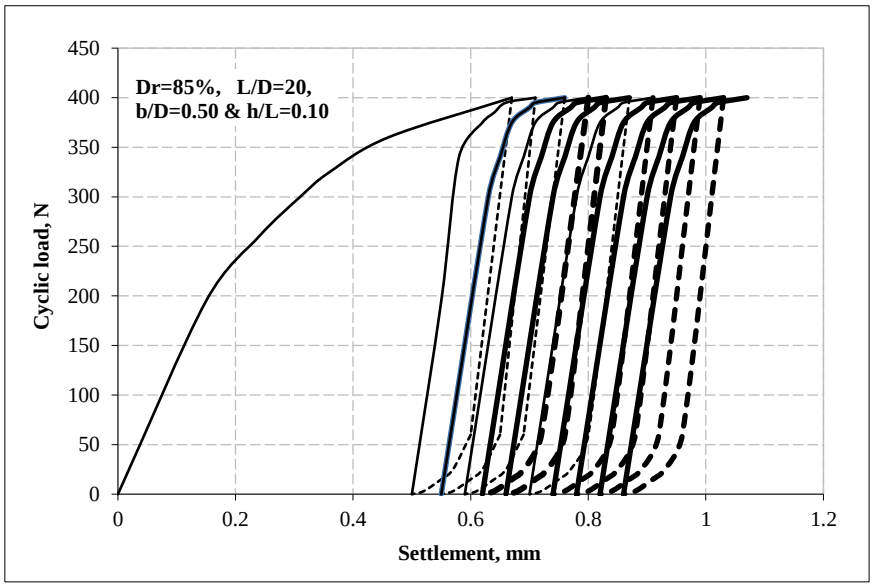

(b)

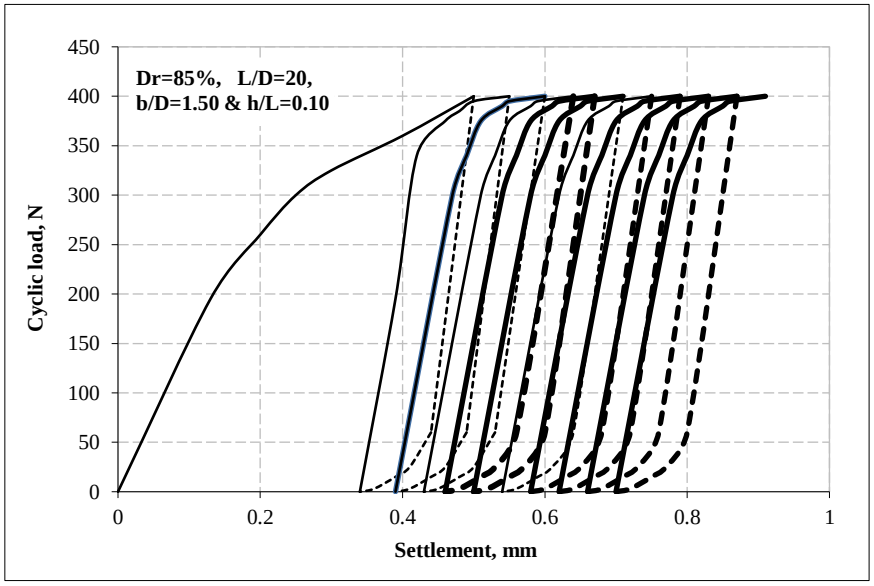

(c)

Figure 11. Variation of pile cap settlement during force-controlled loading cycles: (a) finned pile with fin width ratio 0.50; (b) finned pile with fin width ratio 1.00; (c) finned pile with fin width ratio 1.50

3.2.2. Axial Stiffness

Figure 12 presents the axial load–settlement response of the non-displacement pile under force-controlled cyclic loading with an amplitude of approximately 400 N. The experimental results indicate that greater permanent deformation occurs at the pile tip due to axial cyclic loading for b/D = 0.50 compared to other fin width ratios.

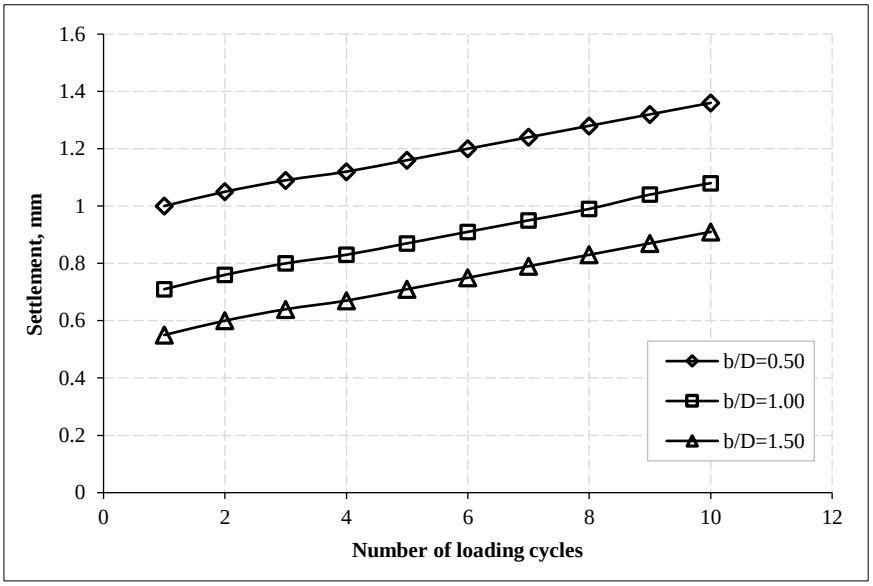

Figure 12. Accumulation of pile head displacement with number of loading cycles-cyclic compression tests

Poulos [34] defined the degradation factor for skin friction, base resistance, and soil modulus as the ratio of the property after cyclic loading to that under static conditions, to quantify the effects of soil degradation. El Naggar & Sakr [35] and Fahmy & El Naggar [36] introduced the axial stiffness factor (K) to evaluate the effect of cyclic loading on pile stiffness, as follows:

$$K = \frac{P_{max} - P_{min}}{\delta_{max} - \delta_{min}} \quad (2)$$

where, P_{max} and P_{min} are the maximum and minimum applied loads during each load cycle, δ_{max} and δ_{min} are the corresponding maximum and minimum displacements, respectively, excluding the permanent settlement accumulated in previous cycles. Soil underneath the pile tip is densified then its stiffness increases gradually with the axial load cycling and pile axial stiffness increases with increase fin width ratio.

3.3. Scale Effect

To study the effect of boundary conditions of the cylindrical tank and the extent of the active zone around the modeled pile, six linear displacement transducers (LDTs) were used to measure pile settlement and vertical settlement of the soil surface. Two LDTs were used to measure pile head movement (upward and downward), while four LDTs were positioned at distances of 2D, 4D, 6D, and 8D from the pile centerline. The boundary effect was evaluated in terms of relative settlement, defined as the ratio between the vertical settlement of the soil surface and the pile settlement at ultimate load. At a distance of 8D, the vertical settlement of the soil surface was equal to zero. The average values of relative settlement were 0.04, 0.006, and 0.001 at distances of 2D, 4D, and 6D from the pile centerline, respectively. These values indicate that the boundary conditions had a minor effect on the results obtained from the physical model.

To minimize boundary effects, the side distance between the tank boundary and the pile perimeter was set to 9D. Previous studies, including Robinsky & Morrison [37], Nazir [38], Shark & Patra [39], Fattah & Al-Soudani [40], Fattah et al. [41, 42], and Al-Suhaily et al. [43], suggest that the distance between the pile tip and the bottom boundary should range from 15D to 30D, which is satisfied in the present model. The ratio of pile diameter (D = 17 mm) to mean grain size (d_{50} = 0.525 mm) exceeds 30, indicating that scale effects can be neglected, as reported by Franke & Muth [44]. Additionally, the surface roughness condition, expressed as $Ra/d_{50} > 0.003$, follows the recommendation of Lings & Dietz [45], where Ra represents the average deviation of roughness heights along the pile surface from the mean line.

3.4. Comparative Study with Other Investigators

Comparison with previous studies shows good agreement. The results are consistent with the work of Uesugi & Kishida [29], who introduced the concept of normalized roughness. They found that when the surface roughness (Ra) exceeds a critical value relative to the mean grain size of the sand (d_{50}), the failure plane shifts from the pile–soil interface into the surrounding soil mass. The results confirm that increasing Ra from 0.15 mm to 0.425 mm improves pile capacity, suggesting that the critical roughness was not fully reached at Ra = 0.15 mm in the tested soil, allowing further increases in friction as roughness increases.

These findings are also consistent with those reported by Peng et al. [46] regarding finned or star-shaped piles. Previous research indicates that fins not only increase surface area but also create a soil-plugging effect. The soil trapped between the fins moves with the pile, effectively increasing the pile diameter to the outer edge of the fins. Figure 7 shows a near-linear increase in load increment (ΔP) with increasing b/D, confirming that a larger trapped soil plug leads to higher bearing capacity. As a result, the pile behaves similarly to a displacement pile with a larger effective diameter. Accordingly, adding fins significantly increases the ultimate load capacity (Pu), particularly as fin length (h/L) and width (b/D) increase.

4. Conclusions

Numerous experimental tests were conducted on densely packed sand supporting the rocket pile, examining three different fin length ratios and three distinct fin width ratios, along with variations in surface roughness and slenderness ratio. The test results lead to the following conclusions:

- The experimental findings indicate that achieving a higher ultimate pile load requires adopting an optimal fin width ratio (b/D) within or above the range of 1.0.
- Pile surface roughness significantly modifies the load–settlement curves and enhances the ultimate pile load.
- The ultimate pile load increases linearly with increasing pile surface roughness until reaching a peak at Ra = 0.08 mm.
- The ultimate pile load is considerably higher when fins are positioned at the pile tip compared to the pile top, with an increase ranging from 2 to 4 times.
- Similarly, the ultimate pile load is higher when fins are positioned at the pile tip compared to the pile middle, with an increase ranging from 1.5 to 3 times.
- The stiffness of the soil surrounding the pile shaft, as observed during cyclic compression testing of finned piles, increases with increasing fin width ratio.

5. Nomenclature

L	Pile embedded depth	Lf	Fin length
D	Pile external diameter	b	Fin width
N	Number of cycles	Dr	Relative density
Ao	Axial cyclic load amplitude	d50	Soil median particle size
Pmax	Maximum axial cyclic load	Ra	Surface roughness
Pmin	Minimum axial cyclic load	Lr	Load ratio
Po	Mean axial cyclic load	t	Time
F	Frequency of cycles	T	Cyclic period
Pu static	Ultimate pile capacity under static load	Pu cyclic	Ultimate pile capacity after 10 cyclic

6. Declarations

6.1. Author Contributions

Conceptualization, M.B., W.A., and A.B.; methodology, M.E., W.A., and A.B.; formal analysis, M.E. and W.A.; investigation, M.E., W.A., and A.B.; resources, M.E. and A.B.; writing—original draft preparation, M.E., W.A., and A.B.; writing—review and editing, M.E., W.A., and A.B. All authors have read and agreed to the published version of the manuscript.

6.2. Data Availability Statement

The data presented in this study are available on request from the corresponding author.

6.3. Funding

The authors received no financial support for the research, authorship, and/or publication of this article.

6.4. Conflicts of Interest

The authors declare no conflict of interest.

6.5. Competing Interests

The authors wish to confirm that there are no known conflicts of interest associated with this publication and there has been no significant financial support for this work that could have influenced its outcome.

7. References

[1] El Naggar, M. H., & Wei, J. Q. (1999). Axial capacity of tapered piles established from model tests. Canadian Geotechnical Journal, 36(6), 1185–1194. doi:10.1139/t99-076.

[2] Ghazavi, M. (2008). Response of tapered piles to axial harmonic loading. Canadian Geotechnical Journal, 45(11), 1622–1628. doi:10.1139/t08-073.

[3] Lee, P. Y., & Gilbert, L. W. (1980). The behavior of steel rocket shaped pile. Symposium on Deep Foundations, 25 October, 1980, Atlanta, United States.

[4] Chan, S.-F., & Hanna, T. H. (1980). Repeated Loading on Single Piles in Sand. Journal of the Geotechnical Engineering Division, 106(2), 171–188. doi:10.1061/ajgeb6.0000920.

[5] Malik, N., Chen, W.-B., Chen, Z.-J., Wu, P.-C., & Yin, J.-H. (2024). Axial Cyclic and Static Behavior of FRP Composite Seawater–Sea Sand Concrete Piles Ended in a Rock Socket. Journal of Geotechnical and Geoenvironmental Engineering, 150(4), 04024013. doi:10.1061/jggefk.gteng-11529.

[6] Poulos, H. G. (1981). Cyclic Axial Response of Single File. Journal of the Geotechnical Engineering Division, 107(1), 41–58. doi:10.1061/ajgeb6.0001089.

[7] Poulos, H. G. (1988). Cyclic stability diagram for axially loaded piles. Journal of Geotechnical Engineering, 114(8), 877–895. doi:10.1061/(ASCE)0733-9410(1988)114:8(877).

[8] Jardine, R. J., & Standing, J. R. (2000). Pile load testing performed for HSE cyclic loading study at Dunkirk, France (Volume 2): Health and Safety Executive, Report No. OTO-2000-007.

[9] White, D. J., & Lehane, B. M. (2004). Friction fatigue on displacement piles in sand. Geotechnique, 54(10), 645–658. doi:10.1680/geot.2004.54.10.645.

[10] Cuéllar, P., Georgi, S., Baeßler, M., & Rücker, W. (2012). On the quasi-static granular convective flow and sand densification around pile foundations under cyclic lateral loading. Granular Matter, 14(1), 11–25. doi:10.1007/s10035-011-0305-0.

[11] Li, Z., Bolton, M. D., & Haigh, S. K. (2012). Cyclic axial behaviour of piles and pile groups in sand. Canadian Geotechnical Journal, 49(9), 1074–1087. doi:10.1139/T2012-070.

[12] Bhattacharya, S., Nikitas, N., Garnsey, J., Alexander, N. A., Cox, J., Lombardi, D., Muir Wood, D., & Nash, D. F. T. (2013). Observed dynamic soil-structure interaction in scale testing of offshore wind turbine foundations. Soil Dynamics and Earthquake Engineering, 54, 47–60. doi:10.1016/j.soildyn.2013.07.012.

[13] Lombardi, D., Bhattacharya, S., & Muir Wood, D. (2013). Dynamic soil-structure interaction of monopile supported wind turbines in cohesive soil. Soil Dynamics and Earthquake Engineering, 49, 165–180. doi:10.1016/j.soildyn.2013.01.015.

[14] Thomassen, K., Ibsen, L. B., & Andersen, L. V. (2017). Laboratory test setup for cyclic axially loaded piles in sand. Electronic Journal of Geotechnical Engineering, 22(3), 1089-1106.

[15] Azzam, W. R., & Elwakil, A. Z. (2017). Model Study on the Performance of Single-Finned Pile in Sand under Tension Loads. International Journal of Geomechanics, 17(3), 4016072. doi:10.1061/(asce)gm.1943-5622.0000761.

[16] Sakr, M., Nazir, A., Azzam, W., & Sallam, A. (2020). Model study of single pile with wings under uplift loads. Applied Ocean Research, 100, 102187. doi:10.1016/j.apor.2020.102187.

[17] Ramadan, N. O., Nasr, A. M., & Azzam, W. R. (2023). Model study of the geotechnical behavior of a single pile under torsional load in contaminated sand. Arabian Journal of Geosciences, 16(12), 674. doi:10.1007/s12517-023-11793-4.

[18] Nasr, A. M., Azzam, W. R., & Khater, A. I. (2024). Experimental studies on the response of single-finned pile under combined vertical-torsional loads in sand. Geomechanics and Geoengineering, 19(4), 586–604. doi:10.1080/17486025.2023.2296060.

[19] Sallam, A., Nasr, A., & Azzam, W. (2024). Effects of Simultaneous Torsional and Lateral Loads on Shaft Piles with Fins in Sandy Soil. Geotechnical and Geological Engineering, 42(5), 3777–3803. doi:10.1007/s10706-024-02757-w.

[20] Nazir, A., Azzam, W., Farouk, A., Nasr, A., & Aamer, F. (2024). Pullout Response of the Pre-displacement Bladed Anchor in Cohesionless Soil. International Journal of Geosynthetics and Ground Engineering, 10(2), 25. doi:10.1007/s40891-024-00530-w.

[21] Sakr, M. A., Azzam, W. R., & Wahba, M. A. (2020). Model study on the performance of single-finned piles in clay under lateral load. Arabian Journal of Geosciences, 13(4), 1–13. doi:10.1007/s12517-020-5068-7.

[22] Hagemann, A., Bienen, B., O'Loughlin, C., & Grabe, J. (2025). The response of pile foundations in sand to axial cyclic loading. 5th International Symposium on Frontiers in Offshore Geotechnics (ISFOG 2025), 9-13 June, 2025, Nantes, France.

[23] Zhou, P., Dai, F., He, B., Liu, Y., Yang, S., & Wei, M. (2025). Experimental investigation on the axial static and cyclic response of a single pile in medium-dense sands. Applied Ocean Research, 156, 104256. doi:10.1016/j.apor.2025.104493.

[24] ASTM D422-63(2007). (2014). Standard Test Method for Particle-Size Analysis of Soils. ASTM International, Pennsylvania, United States. doi:10.1520/D0422-63R07 .

[25] ASTM D3080/D3080M-11. (2020). Standard Test Method for Direct Shear Test of Soils Under Consolidated Drained Conditions. ASTM International, Pennsylvania, United States. doi:10.1520/D3080_D3080M-11.

[26] Sakr, M. A., Nazir, A. K., Azzam, W. R., & Sallam, A. F. (2016). Behavior of grouted single screw piles under inclined tensile loads in sand. Electronic Journal of Geotechnical Engineering, 21(2), 571–592.

[27] Basha, A., & Azzam, W. R. (2018). Uplift Capacity of Single Pile Embedded in Partially Submerged Sand. KSCE Journal of Civil Engineering, 22(12), 4882–4890. doi:10.1007/s12205-017-1715-2.

[28] Azzam, W. R., & Basha, A. M. (2018). Utilization of micro-piles for improving the sub-grade under the existing strip foundation: experimental and numerical study. Innovative Infrastructure Solutions, 3(1), 44. doi:10.1007/s41062-018-0149-0.

[29] Uesugi, M., & Kishida, H. (1986). Influential Factors of Friction Between Steel and Dry Sands. Soils and Foundations, 26(2), 33–46. doi:10.3208/sandf1972.26.2_33.

[30] Blanc, M., & Thorel, L. (2016). Effects of cyclic axial loading sequences on piles in sand. Geotechnique Letters, 6(2), 163–167. doi:10.1680/jgele.15.00155.

[31] Terzaghi, K. (1943). Theoretical Soil Mechanics. John Wiley & Sons, Hoboken, United States. doi:10.1002/9780470172766.

[32] ASTM D1143/D1143M-20. (2024). Standard Test Methods for Deep Foundation Elements Under Static Axial Compressive Load. ASTM International, Pennsylvania, United States. doi:10.1520/D1143_D1143M-20 .

[33] Butler, H. D., & Hoy, H. E. (1977). Users package for the computer storage and analysis of static pile load test data. Federal Highway Administration (FHWA), Washington, United States.

[34] Poulos, H. G. (1989). Cyclic axial loading analysis of piles in sand. Journal of Geotechnical Engineering, 115(6), 836–852. doi:10.1061/(ASCE)0733-9410(1989)115:6(836).

[35] El Naggar, M. H., & Sakr, M. (2002). Cyclic Response of Axially Loaded Tapered Piles. International Journal of Physical Modelling in Geotechnics, 2(4), 1–12. doi:10.1680/ijpmg.2002.2.4.01.

[36] Fahmy, A., & El Naggar, M. H. (2016). Cyclic axial performance of helical-tapered piles in sand. DFI Journal, 10(3), 98–110. doi:10.1080/19375247.2016.1211353.

[37] Robinsky, E. I., & Morrison, C. F. (1964). Sand Displacement and Compaction around Model Friction Piles. Canadian Geotechnical Journal, 1(2), 81–93. doi:10.1139/t64-002.

[38] Nazir, A. K. (2008). Effect of installation method in uplift capacity of piles in sand. Alexandria Engineering Journal, 23(3), 156-167.

[39] Shelke, A., & Patra, N. R. (2009). Effect of arching on uplift capacity of single piles. Geotechnical and Geological Engineering, 27(3), 365–377. doi:10.1007/s10706-008-9236-x.

[40] Hussein, B. S., Rahil, F. H., & Al-Neami, M. A. M. (2016). Bearing Capacity of Closed and Open Ended Pipe Piles in Clayey Soil. Engineering and Technology Journal, 34(8), 1615–1623. doi:10.30684/etj.34.8a.12.

[41] Fattah, M. Y., Al-Soudani, W. H., & Omar, M. (2016). Estimation of bearing capacity of open-ended model piles in sand. Arabian Journal of Geosciences, 9(3), 242. doi:10.1007/s12517-015-2194-8.

[42] Fattah, M. Y., Zbar, B. S., & Mustafa, F. S. (2021). Effect of soil saturation on load transfer in a pile excited by pure vertical vibration. Proceedings of the Institution of Civil Engineers: Structures and Buildings, 174(2), 132–144. doi:10.1680/jstbu.16.00206.

[43] Al-Suhaily, A. S., Abood, A. S., & Fattah, M. Y. (2018). Bearing Capacity of Uplift Piles with End Gates. Proceedings of China-Europe Conference on Geotechnical Engineering. Springer Series in Geomechanics and Geoengineering, Springer, Cham, Switzerland. doi:10.1007/978-3-319-97115-5_3.

[44] Franke, E., & Muth, G. (1985). Scale effect in 1g model tests on horizontally loaded piles. Proceedings of the 11th International Conference on Soil Mechanics and Foundation Engineering, 12-16 August, 1985, San Francisco, United States. (In French).

[45] Linos, M. L., & Dietz, M. S. (2005). The peak strength of sand-steel interfaces and the role of dilation. Soils and Foundations, 45(6), 1–14. doi:10.3208/sandf.45.1.

[46] Peng, J. R., Rouainia, M., & Clarke, B. G. (2010). Finite element analysis of laterally loaded fin piles. Computers and Structures, 88(21–22), 1239–1247. doi:10.1016/j.compstruc.2010.07.002.